PHYSICAL REVIEW MATERIALS **5**, 045601 (2021)

Thin film growth of phase-separating phthalocyanine-fullerene blends: A combined experimental and computational study

Berthold Reisz,[1] Eelco Empting,[1] Matthias Zwadlo,[1] Martin Hodas,[1] Giuliano Duva,[1] Valentina Belova,[1,2]
Clemens Zeiser,[1] Jan Hagenlocher,[1] Santanu Maiti,[1,3] Alexander Hinderhofer,[1] Alexander Gerlach,[1]
Martin Oettel,[1] and Frank Schreiber[1,4]
[1] *Institute for Applied Physics, University of Tübingen, Auf der Morgenstelle 10, 72076 Tübingen, Germany*
[2] *European Synchrotron Radiation Facility, 71, avenue des Martyrs CS 402200, 38043 Grenoble Cedex 9, France*
[3] *Jülich Centre of Neutron Science (JCNS-1), Forschungszentrum Jülich GmbH, 52425 Jülich, Germany*
[4] *Center for Light-Matter Interaction, Sensors & Analytics LISA+, University of Tübingen, Auf der Morgenstelle 15, 72076 Tübingen, Germany*

(Received 26 November 2020; revised 8 March 2021; accepted 16 March 2021; published 5 April 2021)

Blended organic thin films have been studied during the last decades due to their applicability in organic solar cells. Although their optical and electronic features have been examined intensively, there is still a lack of detailed knowledge about their growth processes and resulting morphologies, which play a key role in the efficiency of optoelectronic devices such as organic solar cells. In this study, pure and blended thin films of copper phthalocyanine (CuPc) and the Buckminster fullerene (C_{60}) were grown by vacuum deposition onto a native silicon oxide substrate at two different substrate temperatures, 310 and 400 K. The evolution of roughness was followed by *in situ* real-time x-ray reflectivity. Crystal orientation, island densities, and morphology were examined after the growth by x-ray diffraction experiments and microscopy techniques. The formation of a smooth wetting layer followed by rapid roughening was found in pure CuPc thin films, whereas C_{60} shows a fast formation of distinct islands at a very early stage of growth. The growth of needlelike CuPc crystals losing their alignment with the substrate was identified in co-deposited thin films. Furthermore, the data demonstrate that structural features become larger and more pronounced and that the island density decreases by a factor of four when going from 310 to 400 K. Finally, the key parameters roughness and island density were well reproduced on a smaller scale by kinetic Monte Carlo simulations of a generic, binary lattice model with simple nearest-neighbor interaction energies. A weak molecule-substrate interaction caused a fast island formation and weak interaction between molecules of different species was able to reproduce the observed phase separation. The introduction of different same-species and cross-species Ehrlich-Schwoebel barriers for interlayer hopping was necessary to reproduce the roughness evolution in the blend and showed the growth of CuPc crystals on top of the thin film in agreement with the experiment.

DOI: 10.1103/PhysRevMaterials.5.045601

I. INTRODUCTION

Organic semiconductors are a class of materials, which offer a wide range of possibilities for basic research and technical applications. For this purpose, thin films of small-molecule organic semiconductors have been studied during the last decades by means of evaporation in vacuum, which provides both layer thickness control and a clean environment [1–3]. Binary blends of small organic molecules serving as donor-acceptor systems in photovoltaic cells represent one of the technical applications. In particular, many small organic molecules co-evaporated with the well known Buckminster fullerene C_{60} exhibit phase separation [4]. It was shown that the degree of phase separation and the resulting thin film architecture play a key role for the solar cell efficiency due to the diffusion and dissociation of excitons at donor-acceptor interfaces [5–8]. There are many studies on the optical properties and solar cell efficiencies, but the evolution of the underlying thin film architectures by self-assembly phenomena is not yet fully understood. Prior studies already attempted to assign structural features to pure domains in phase separated blends containing the Buckminster fullerene (C_{60}) together with other organic compounds such as sexithiophene (6T) [9,10], diindenoperylene (DIP) [11,12], pentacene (PEN) [13], and copper phthalocyanine (CuPc) [14,15], but the desired assignment remained unclear. Only for PEN, it was possible to conclude from the width of x-ray reflectivity peaks that it forms islands with a height exceeding the nominal film thickness. The present study shows needlelike CuPc-crystals protruding from blended CuPc-C_{60} thin films. Furthermore, it investigates the growth of pure and blended CuPc-C_{60} thin films, both experimentally and by simulations. The experiments examine the growth up to a film thickness of approximately 20 nm in real-time and *in situ* during the growth at two different substrate temperatures, 310 and 400 K, as well as *in* and *ex situ* after the growth. The simulations are performed within a generic, two-species lattice model considering structure formation by particle diffusion as it was studied for atomic thin films in the past [16,17]. Qualitative agreement between simulations and experiments

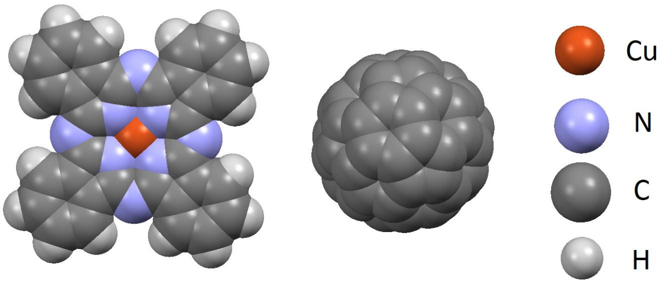

FIG. 1. (Left) Copper phthalocyanine ($CuN_8C_{32}H_{16}$, abbrev. CuPc). (Right) Buckminster Fullerene (C_{60}, abbrev. C_{60}).

has been achieved, which gives evidence for the usefulness of such simple models to describe actual experiments. From the general perspective of structure formation in thin films, the CuPc-C_{60} system is a model system for phase separation. Film height and time-dependent phase ordering enter as new aspects compared to single-component film growth. It can be expected that phase ordering also influences island distribution and roughness. General considerations on large length scales indicate that also phase-separating binary mixtures exhibit Kardar-Parisi-Zhang (KPZ) scaling [18,19], but little is known on smaller length scales. Simulations on micro- to mesoscopic length scales are not abundant. On the one hand, there are a few studies on molecular dynamics taking all atoms into account. Those studies attempt to model faithfully the growth process of a specific molecule, but are generically limited by the small number of particles and the necessity to consider much higher deposition rates for computational reasons. Examples are pentacene (PEN) growth on C_{60} [20] or silica [21] and 6T monolayer growth on SiO_x [22]. Typically, one would use simpler, generic lattice models to bridge the microscopic and the mesoscopic scale. In the literature, such models have been used mainly to discuss epitaxial growth of pure thin films, i.e., consisting of only one particle species, either for submonolayers [23], or the 3D growth of mounds [24–27]. Early extensions to binary systems can be found in Refs. [28,29]. Here, we will apply a binary model on a cubic lattice to the CuPc-C_{60} system and focus on roughness and island densities as observables to compare with the experiments. An important question is whether general trends in these observables as a function of composition and temperature can be explained by the lattice model with its generic parameters. This paper is organized as follows. In Secs. II and III, more details about the methods used in experiment and simulation are given. Section IV presents results for which a meaningful comparison between experiments and simulations is possible: film roughness, island densities and real-space images. Finally, Sec. V gives a summary and conclusions.

II. EXPERIMENTS

A. Preparation of organic thin films

Copper phthalocyanine (CuPc) and the Buckminster fullerene (C_{60}), were purchased from Sigma Aldrich (purity 99.9 % by gradient sublimation), see Fig. 1. Native silicon oxide substrates were cleaned by acetone and then by isopropanol in an ultrasonic bath for 5 minutes each. Afterwards, the substrates were installed inside a vacuum chamber for organic molecular beam deposition and heated up to 500 K for 10 hours until a vacuum in the pressure range of 10^{-9} mbar was achieved. Pure and blended thin films containing CuPc and C_{60} were deposited onto the substrates at two different substrate temperatures, 310 and 400 K. The blends were prepared by simultaneous evaporation of CuPc and C_{60} at a molar mixing ratio of 1:1, which is known as co-deposition and was applied in order to investigate the phase separation. Phase separation is an intrinsic property of the CuPc-C_{60} system and co-deposition excludes any external effects that may contribute to it. Sequential deposition for instance is another preparation technique and means that a pure layer of species A is grown in advance and afterwards, a second layer of species B is grown on top of it. The separation into pure layers is then a result of the preparation technique, whereas co-deposition does not force a separation. For a better comparison between pure and blended thin films, we calibrated the evaporation temperatures of the individual effusion cells in advance such that a total deposition rate of 2.0 Å/min was maintained for 100 min for both, pure and blended thin films.

B. In situ experiments

For the purpose of *in situ* x-ray diffraction experiments during and after the growth, a portable ultrahigh vacuum chamber for organic molecular beam deposition equipped with a 360°-beryllium window was used [30–32]. The *in situ* real-time and post-growth x-ray reflectivity scans (XRR), as well as the *in situ* post-growth grazing incidence x-ray diffraction scans (GIXD) were carried out at the material science beamline for surface analysis MS-X04SA of the Swiss Light Source using synchrotron radiation with an energy of 12.7 keV [33]. The grazing angle of incidence in GIXD was chosen close to the total reflection edge of silicon such that the x-ray beam probed the samples throughout the entire film thickness.

C. Real-time XRR

The measured intensities $I(q,t)$ of all real-time XRR scans (q is the momentum transfer and t the time) are shown in Fig. 2. Previous studies investigated the evolution of roughness by recording the reflected x-ray intensities at specific q_z values during the growth of pure films. Those q_z values are the anti-Bragg point $^1/_2 \cdot q_{\text{Bragg}}$ and $^2/_3$, $^3/_4$, $^4/_5$, and $^5/_6$ of q_{Bragg} [12,34–41]. Due to the absence of a clear Bragg peak in the XRR-scans of pure C_{60} and the blended thin films there are no anti-Bragg points to be observed. Instead, full XRR scans up to $q_z \approx 0.6$ Å^{-1} were carried out and the evolution of the root mean square roughness σ was determined from the damping of Kiessig oscillations in the low q_z range. The software GENX, which is based on the Parratt formalism [42], was applied for fitting the Kiessig oscillations up to 0.15 Å^{-1} for pure C_{60} and up to 0.20 Å^{-1} for pure CuPc and the blend. For simplicity, the thin films were assumed to be homogeneous with a gradual decrease of the electron density in z direction, which simulates the surface roughness. A thin void layer was inserted in the model between substrate and organic film in order to simulate the electron density at the interface. Thickness and roughness of the void layer were fitted by the software GENX. The XRR

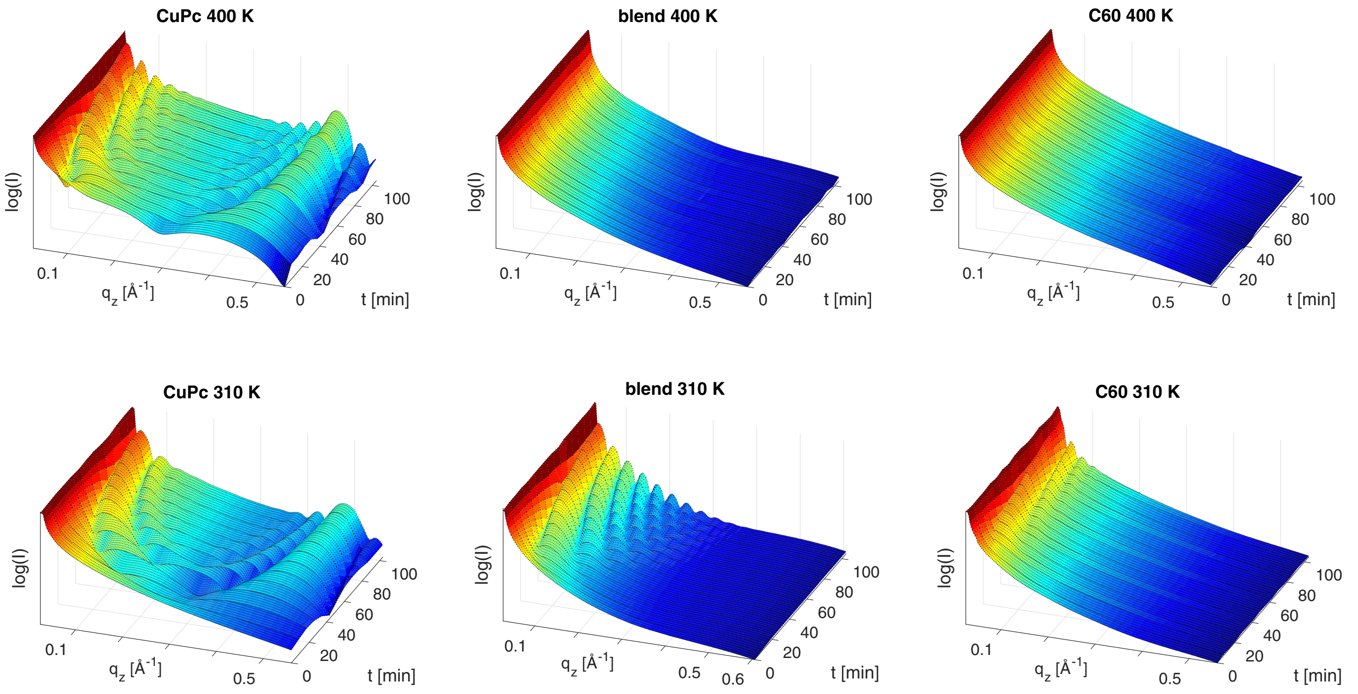

FIG. 2. X-ray reflectivity (XRR) of pure CuPc (left), pure C_{60} (right) and a 1:1 blend of both molecules (middle) measured *in situ* and in real-time during the growth at two different substrate temperatures: 310 (bottom row) and 400 K (top row). The profiles of pure C_{60} and the 1:1 blend grown at 400 K exhibit no Kiessig oscillations, which means that those two films are already rough from the beginning of growth.

scans of the pure C_{60} and the blended thin film grown at 400 K exhibit no Kiessig oscillations due to a pronounced roughness throughout the entire film growth. Hence, the evolution of roughness was determined only for the thin films grown at 310 K.

D. Post-growth XRR

Figure 3(a) shows the *in situ* post-growth x-ray reflectivity scans (XRR). The roughness σ of each thin film was determined from the damping of Kiessig oscillations in the low q_z range as described above. The lattice spacing in out-of-plane direction was determined for CuPc from the q_z values of Bragg peaks and was around 13 Å at both substrate temperatures.

E. Post-growth GIXD

Figure 3(b) shows the *in situ* post-growth grazing incidence x-ray diffraction scans (GIXD) after transformation into the reciprocal q_{xy} space. Crystal structures were determined from q_{xy} values and the corresponding Bragg peaks were indexed

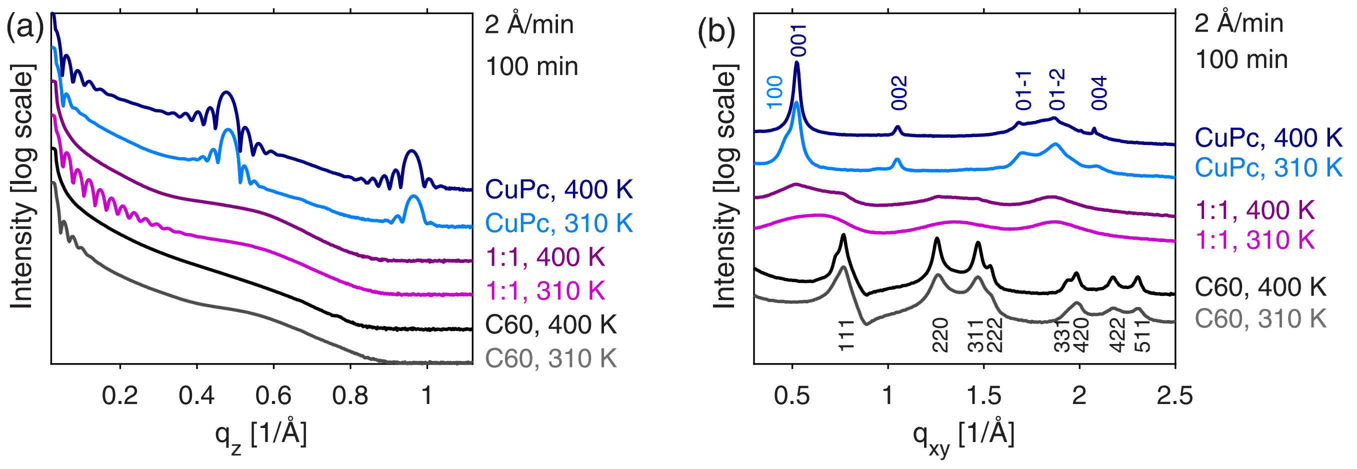

FIG. 3. (a) X-ray reflectivity scans (XRR). The influence of mixing and substrate temperature on the roughness is clearly recognizable from the number of visible Kiessig oscillations in the low q_z range. The vanishing of CuPc Bragg peaks in the blends indicates that the presence of C_{60} hinders the spatial alignment of CuPc crystals with the substrate surface. (b) Grazing incidence x-ray diffraction (GIXD): the presence of CuPc and C_{60} peaks in the profiles of the blended thin films proves their phase separation. The peak broadening indicates that the lateral sizes of coherently scattering domains became smaller in the blends.

accordingly to the literature [43–47]. Occasionally, several (hkl) reflections contribute to the same Bragg peak. For those Bragg peaks containing multiple (hkl) triplets, only one triplet is indicated for clarity. The lateral size of coherently scattering domains d_{coh} was estimated from the GIXD diffraction patterns by fitting the full width at half of maximum (FWHM) of the (001) peak for CuPc and the (111) peak for C_{60} due to the Scherrer formula $d_{\text{coh}} \approx K\,2\pi/\Delta q_{\text{FWHM}}$ with shape factor $K \approx 1$, which is in between the value $K = 0.93$ for N ideal (i.e., infinitely wide) lattice planes and $K = 1.11$ for perfectly spherical domains [48]. We consider the mean value of $K \approx 1$ as a suitable estimate for domains whose shape varies between spherical and extremely elongated. The fitted Gauss curves and the corresponding fit parameters are shown in Fig. S1 in Ref. [49].

F. Reciprocal space maps

A second set of samples was prepared under the same conditions for *ex situ* characterization. Reciprocal space maps of those samples were acquired at the beamline ID03 of the European Synchrotron Radiation Facility (ESRF) using synchrotron radiation with an energy of 24.0 keV. The grazing angle of incidence was half of the total reflection angle of silicon such that the measurement was more surface sensitive. The reciprocal space maps are shown in Fig. 4 and served to determine the crystal orientation.

G. AFM, SEM, and HIM images

Real-space images of this second set of samples were obtained by *ex situ* atomic force microscopy (AFM) using a JPK Nanowizard II instrument operating in tapping mode under ambient conditions. The islands were automatically counted for the determination of island densities. The post-growth roughness σ was evaluated by $\sigma = \sqrt{\langle h^2\rangle - \langle h\rangle^2}$ and compared to the root mean square roughness σ determined from post-growth XRR. $h \equiv h(x, y)$ is the height of the film at the lateral position (x, y) in the AFM images. The data were complemented by scanning electron microscopy (SEM) at different magnifications using an XL30-device from Philips at a beam energy of 20 keV and by helium ion microscopy (HIM) using an ORION Nanofab-device from Zeiss at an acceleration voltage of 30 kV. Selected SEM images of the blended thin films are compiled in Ref. [49] (Fig. S2). Selected AFM- and HIM-images in comparison to simulated height maps and 3D snapshots of the simulated growth will be presented and discussed in Sec. IV A below.

H. Experimental evidence of phase separation

The expected phase separation is confirmed by the presence of both CuPc and C_{60} Bragg peaks in the GIXD profiles of blended thin films, see Fig. 3(b). The peak widths are significantly broadened compared to the GIXD peaks of pure films and the corresponding size of coherently scattering domains is less than 4 nm in the blends. This structure was referred to as nanocrystalline in previous studies on phthalocyanine-fullerene blends [50]. For comparison, the lateral size of coherently scattering domains in the pure films increases from 21 to 31 nm for CuPc and from 13 to 22 nm for C_{60} when raising the temperature from 310 to 400 K, see Fig. S1 in Ref. [49]. We see that not only mixing influences the domain sizes, but also changing the substrate temperature. Larger domains are expected at elevated substrate temperatures due to a faster molecular diffusion. Note that pure CuPc and pure C_{60} domains in blended thin films may consist of several nanocrystals with different orientations, which implies that the pure domains might be significantly larger than the size of coherently scattering crystals. Finally, no new Bragg peaks appear in the blends and hence no new crystal structures are formed. The (422) and (511) peaks of C_{60} are not discernible in the blends, mainly due to a substantial peak broadening. Since all peaks are broadened in the blends, the lowest peaks disappear fully, whereas the largest peaks remain visible.

The orientation of crystals was derived from the reciprocal space maps, see Fig. 4. The C_{60} crystals have no preferential orientation with respect to the substrate surface, which leads to concentric rings in the reciprocal space and to the absence of Bragg peaks in the XRR profiles, see Fig. 3(a). The random orientation of C_{60} crystals on native silicon oxide and the formation of islands at a very early stage of growth (as it will be discussed in Sec. IV) is in contrast to the growth of C_{60} on mica [38,39]. It seems that the molecule-substrate interaction plays a crucial role in thin film growth and was therefore considered as one of the main parameters in the simulations (see below). Dissimilar to C_{60}, the CuPc crystals prefer to grow in columns along the substrate surface in a 2D powder, which was confirmed by indexing the distinct peaks in the reciprocal space maps of pure CuPc thin films. Such a 2D powder consists of randomly oriented crystals in two dimensions, but is well ordered in the direction perpendicular to the substrate surface, which can be seen by the well pronounced Bragg peaks in the XRR profiles of pure CuPc, see Fig. 3(a). These findings are in good agreement with previous studies of vacuum deposited CuPc on different substrates [51–54]. It should be mentioned that the q_{xy} value of the CuPc (001)-peak in the GIXD profile coincides with the q_{xy} value of the (00 ± 2) peak in the reciprocal space map, which stems from a different CuPc polymorph. It was shown that both polymorphs co-exist in thin CuPc films on native silicon oxide and that a transition from one crystal structure to the other is possible and occurs most likely at the film-air interface after growth [54]. Finally, the reciprocal space map of the blended thin film grown at 400 K exhibits a weak diffraction ring corresponding to the CuPc (100) reflection, which indicates that the CuPc crystals loose their alignment with the substrate and are now randomly oriented in three dimensions. This result is in good agreement with the missing Bragg peaks in the XRR profiles of blends and it is corroborated by the needlelike crystals protruding from the blended thin films (see Fig. 9). Obviously, the needlelike features can be assigned to CuPc crystals due to their columnar growth.

III. SIMULATIONS

The experimental system is quite complicated with regard to the anisotropy of the CuPc molecule and the associated orientational effects. Even for the nearly isotropic C_{60}, growth with different crystal orientations is possible. We model the

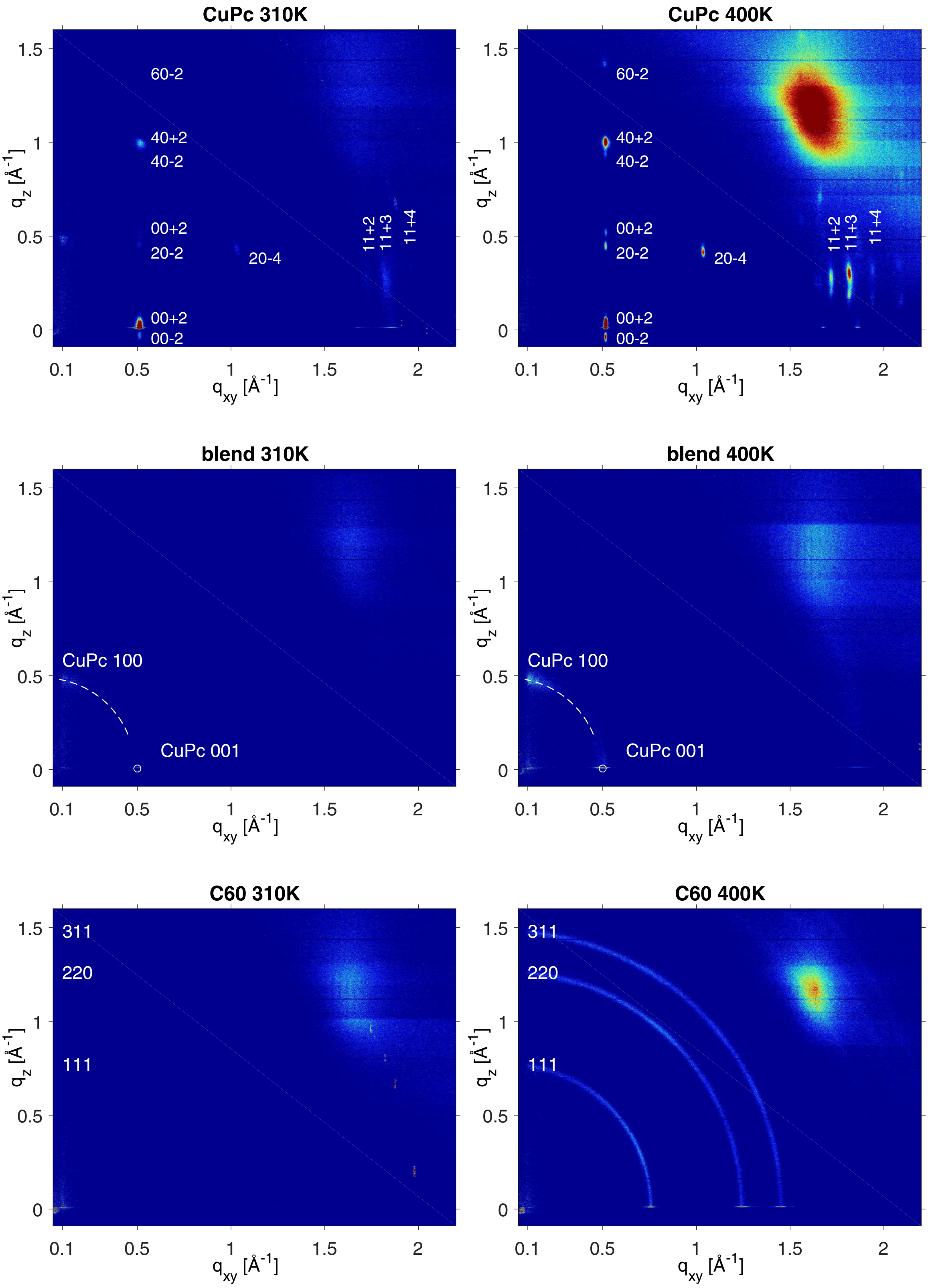

FIG. 4. Reciprocal space maps of CuPc, C_{60}, and blends grown at two different substrate temperatures (310 and 400 K). The bright peak in the upper right corner of each map corresponds to the {111} reflection from the silicon substrate.

system using a rather generic model on a simple cubic lattice in order to focus on the influence of phase separation on roughness and island formation. A guiding principle is to choose parameters to reproduce the roughness behavior seen in the growth process of the pure species and then to explore the effect of phase separation. We employ a simple film growth model using a binary lattice gas (species 1 and 2) on a cubic lattice. Nearest-neighbor particles interact with

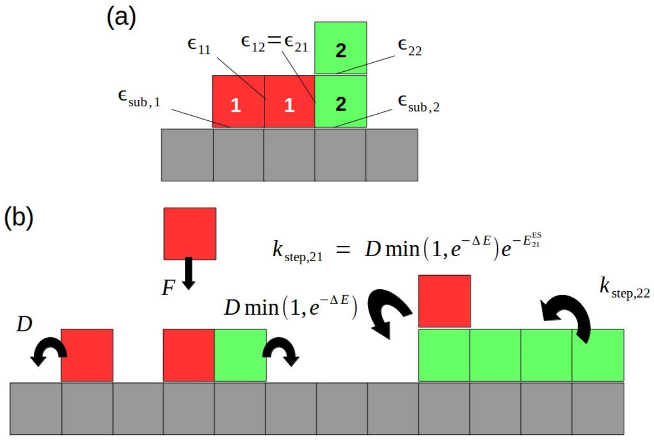

FIG. 5. (a) Interaction energies in the lattice model and (b) allowed lattice moves with their rates.

energies ϵ_{ij} $(i, j = \{1,2\})$ and particles in the first layer have interactions with the substrate (x-y plane) given by $\epsilon_{\mathrm{sub},1}$ or $\epsilon_{\mathrm{sub},2}$. All energies are given in units of $k_BT_0 = 25$ meV ($\approx 4 \times 10^{-21}$ J) and $T_0 = 300$ K. Deposition on top of the film or the bare substrate at random substrate plane coordinates is controlled by a rate F (particles per unit time and lattice site). Diffusion respects the solid-on-solid (SOS) condition [24,25]: only the particles (species i) in the top layer are allowed to diffuse to a lateral next-neighbor site with rate $k = D\min\{1, \exp(-\Delta E)\}$, where $D = k_BT\ \gamma$ is a free diffusion constant and $\gamma \propto e^{-E_D/(k_BT)}$ is a surface mobility with Arrhenius-like temperature dependence featuring a (dimensionful) diffusion barrier E_D. ΔE is the energy difference between final and initial state. In such a diffusion step, particles of species i may also ascend (moving on top of a particle of species j) or descend one layer (moving down from a particle of species j) in which case the rate is multiplied with $\exp(-E_{ij}^{\mathrm{ES}})$ and E_{ij}^{ES} is an Ehrlich-Schwoebel (ES) barrier. Neither overhangs nor desorption are allowed; see Fig. 5 for a compact overview of these definitions. In the one-component case, the model is characterized by the four parameters $\epsilon = \epsilon_{11}$, $\epsilon_{\mathrm{sub}} = \epsilon_{\mathrm{sub},1}$, $E^{\mathrm{ES}} = E_{11}^{\mathrm{ES}}$, and $\Gamma = D/F$. Actual growth experiments of organic thin films are characterized by ϵ between $-15\,k_BT_0$ and $-10\,k_BT_0$ and by Γ between 10^9 and 10^{11}, which is difficult to simulate. Nevertheless, at lower energies and smaller diffusion-to-flux ratios Γ, the model shows similar growth modes as seen experimentally. These are (a) island growth from the start when ϵ_{sub} is low enough, (b) layer-by-layer growth (LBL) and (c) 3D growth of varying degree (For more details on the growth modes and transitions between them in the single-species problem, see Ref. [55]). Matching the single-species growth modes is thus determining our choice of parameters. For CuPc (species 1), 3D growth is observed, which is initially LBL. C_{60} (species 2) exhibits strong island growth. Both growth modes can be approximately modeled by the choices $\epsilon_{11} = -3.0$, $\epsilon_{\mathrm{sub},1} = -2.7$, $E_{11}^{\mathrm{ES}} = 3.0$ (CuPc) and $\epsilon_{22} = -3.0$, $\epsilon_{\mathrm{sub},2} = -1.0$, and $E_{22}^{\mathrm{ES}} = 3.0$ (C_{60}), all in units of k_BT_0. The substrate size is 200×200 sites. We employed (hybrid) kinetic Monte Carlo (KMC) simulations, i.e., the simulation was divided into discrete time steps, during each of which either a new particle was inserted into the box or a move (see above) was attempted for an already existing particle. Insertion happens at a random position (x, y) at a height of $h = \mathrm{height}(x, y) + 1$ and $\mathrm{height}(x, y)$ is the film height at the point (x, y) before insertion. For the other moves, the algorithm would first choose a random site (x, y) at which at least one particle had already been deposited, and then try to move the topmost particle at this site to a random neighboring site. The move is accepted with a probability $p = \min\{1, \exp(-\Delta E)\}$. If the particle has to climb or step down one layer, an additional acceptance probability of $\exp(-E^{\mathrm{ES}})$ applies. This hybrid KMC approach allows us to reduce the amount of bookkeeping necessary to track the change in rates due to the local environment of a particle. On the other hand, of course, this leads to moves being rejected and simulation time being wasted. Whether or not a move is accepted, the simulation time is still incremented by a timestep Δt of variable length (Poisson distributed), since this leads to more accurate dynamics [56]. The interaction energy $\epsilon_{12} = \epsilon_{21}$ and the Ehrlich-Schwoebel barrier $E_{12}^{\mathrm{ES}} = E_{21}^{\mathrm{ES}}$ are cross-species parameters yet to be fixed. CuPc and C_{60} are demixing. For the two-component lattice gas in equilibrium, $2\epsilon_{12} - (\epsilon_{11} + \epsilon_{22}) > 0.88$ leads to demixing, but the deposition dynamics require larger values, otherwise de-mixing is kinetically suppressed. We choose $\epsilon_{12} = -0.5$. For the cross-species Ehrlich-Schwoebel barrier, one might speculate that $E_{12}^{\mathrm{ES}} < E_{11[22]}^{\mathrm{ES}}$ since the introduction of a second species opens more kinetic pathways for a molecule to climb or step down a layer. The presence of lower diffusion barriers facilitates the interlayer diffusion such that $E_{12}^{\mathrm{ES}} < E_{11[22]}^{\mathrm{ES}}$ is justified. Here, we simply choose $E_{12}^{\mathrm{ES}} = 0$. Since $D \propto k_BT\ e^{-E_D/(k_BT)}$, the main control parameter in the model to study the effect of temperature variation is the ratio $\Gamma = D/F$ between diffusion D and flux F. We investigated the values $\Gamma = 10^4$ and 10^5. The change in Γ by a factor of 10 (with $F = \mathrm{const.}$) corresponds to the experimental change in temperature from $T_1 = 310$ K to $T_2 = 400$ K if the diffusion barrier $E_D \approx 11\ k_BT_1$, which is a reasonable value. The roughness σ of a growing film was evaluated in the same way as it was described in the experimental section as $\sigma = \sqrt{\langle h^2\rangle - \langle h\rangle^2}$ with $h \equiv h(x, y)$ as the instantaneous height of the film at the lateral lattice position (x, y). Finally, we note that the simulations were stopped immediately after a predetermined amount of material had been deposited, without time for the structures to equilibrate. This is in contrast to AFM measurements of grown films, which are often performed several days after growth, allowing the structure to potentially undergo changes.

IV. COMPARISON AND DISCUSSION OF RESULTS

A. Real-space images and overall morphology

Typical AFM images are shown in Fig. 6. The distribution of heights is plotted on the right side of each image together with the color bar. Note that the lowest point of the image is set to 0 nm, which is not necessarily the substrate. There might be further completely filled layers of organic molecules below 0 nm and hence the maximum height in the color bar is not necessarily the film thickness. As a result of the molecular structure, C_{60} forms round islands while the anisotropic CuPc molecules assemble in wormlike islands. The increased islands size together with the reduced island density is clearly

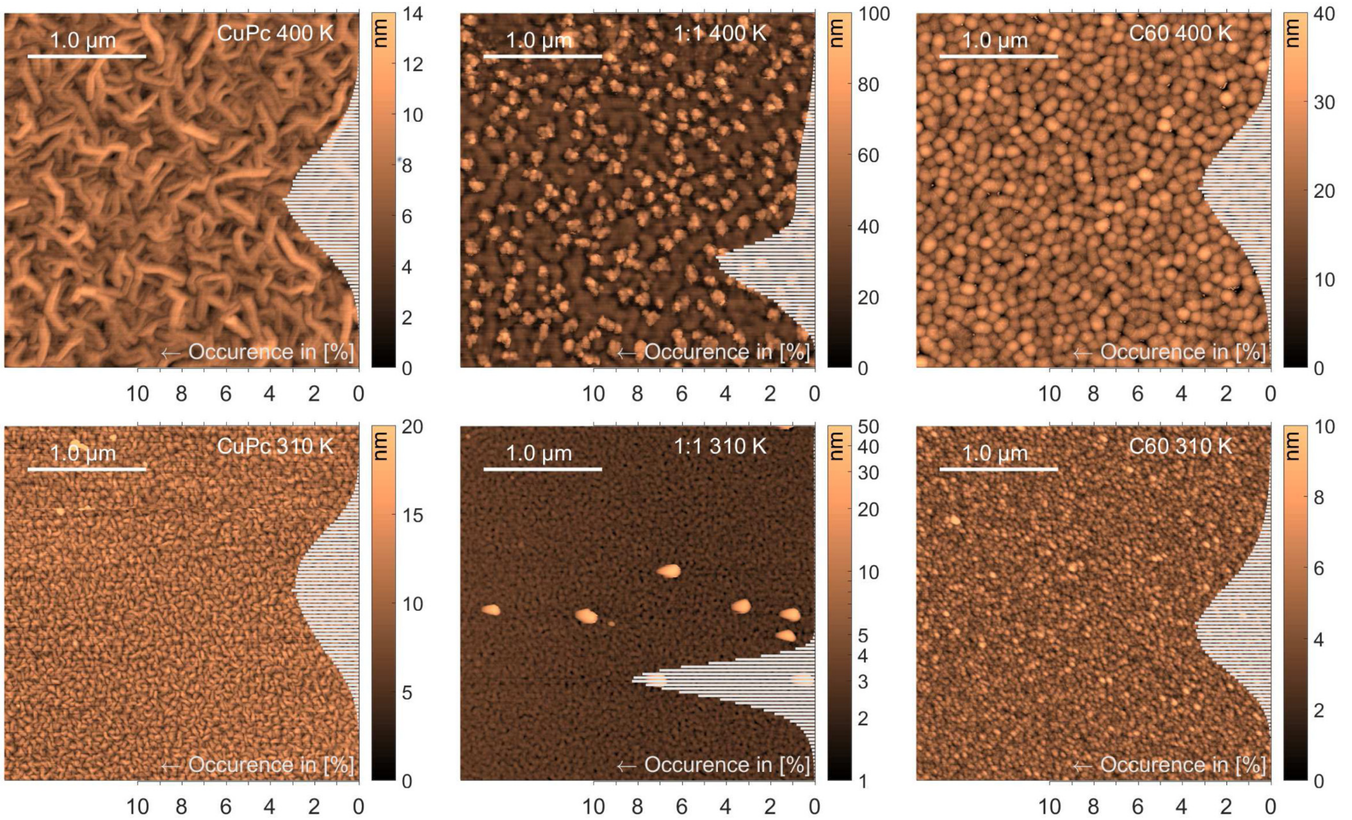

FIG. 6. AFM images (3 μm × 3 μm) of pure CuPc (left), pure C_{60} (right) and the 1:1-blend (middle) grown at 2 Å/min for 100 min (average thickness ≈20 nm) at two different substrate temperatures 310 K (lower row) and 400 K (upper row). The distribution of heights are shown together with the color bar on the right side of each image.

visible at 400 K. A faster diffusion of molecules can be assumed as reason for the increase of island sizes at elevated substrate temperatures. A few tall islands arise in the mixed film at 310 K and their number increases substantially when going to 400 K.

The corresponding simulated height maps after deposition of 20 monolayers are shown in Fig. 7. In a pure system of species 2 (C_{60}), we see that there are "'holes" in the film which reach in some cases down to the substrate (see the right column). This is an artifact of the simulation method, since once the islands of the species merge, these holes occur due to the islands not being perfect squares. In order to fill the holes, new particles have to be deposited inside them, since they are too deep for surrounding particles to hop down and fill them up. In contrast to species 2 (C_{60}), we see how the pure growth of species 1 (CuPc) leads to a very smooth film with no holes. At higher Γ, we see a maximum deviation of ±3 MLs from the mean height of this simulated thin film. Although the lateral length scale in the simulations is much lower when compared to the AFM images, there is qualitative agreement with the experiments regarding the reduction of island densities upon increasing T (or Γ). Clearly, the simulations cannot capture the appearance of the wormlike CuPc islands or the rare tall islands in the mixed film. Instead, the simulations give a time-resolved picture of the 3D structure formation of the film. Example snapshots for the mixed film at the two values of Γ and after deposition of 2, 8, and 20 monolayers are shown in Fig. 8. In the following, the results from the analysis of the time-resolved 3D structure are discussed. In the 1:1 blend, tall islands emerge on top of the film when increasing Γ from 10^4 to 10^5, which are reminiscent of those seen in the experiments at 400 K.

The formation process of these tall islands can be clearly seen in the snapshots of Fig. 8 (upper row). At first, species 2 (C_{60}) will form islands on top of a wetting film of species 1 (CuPc). These islands then serve as nucleation points for clusters of species 1 which grow on top of them. On those, in turn, new clusters of species 2 will grow and this process may be continued.

The simulation of the blended thin films gives rise to further questions to the experimental system. How does the phase separation take place and which features belong to which molecule, i.e., to CuPc or to C_{60}? To answer this question, more insight is given by high resolution helium ion microscopy (HIM) images. Needlelike CuPc crystallites protrude from the blended thin films, see Fig. 9, for example. A previous study reported protruding needles in pure, vapor deposited CuPc films on silicon oxide at larger film thicknesses of 50–500 nm [57]. It appears possible that the CuPc crystals are forced to grow vertically if they are no longer exposed to the bare substrate, i.e., if they grow on already existing film layers. Additional SEM images of blended thin films at different magnifications are compiled in Fig. S2 in Ref. [49]. At low magnifications, those images provide an overview over a large area and prove the homogeneous distribution of tall islands. At high magnifications, the SEM images show

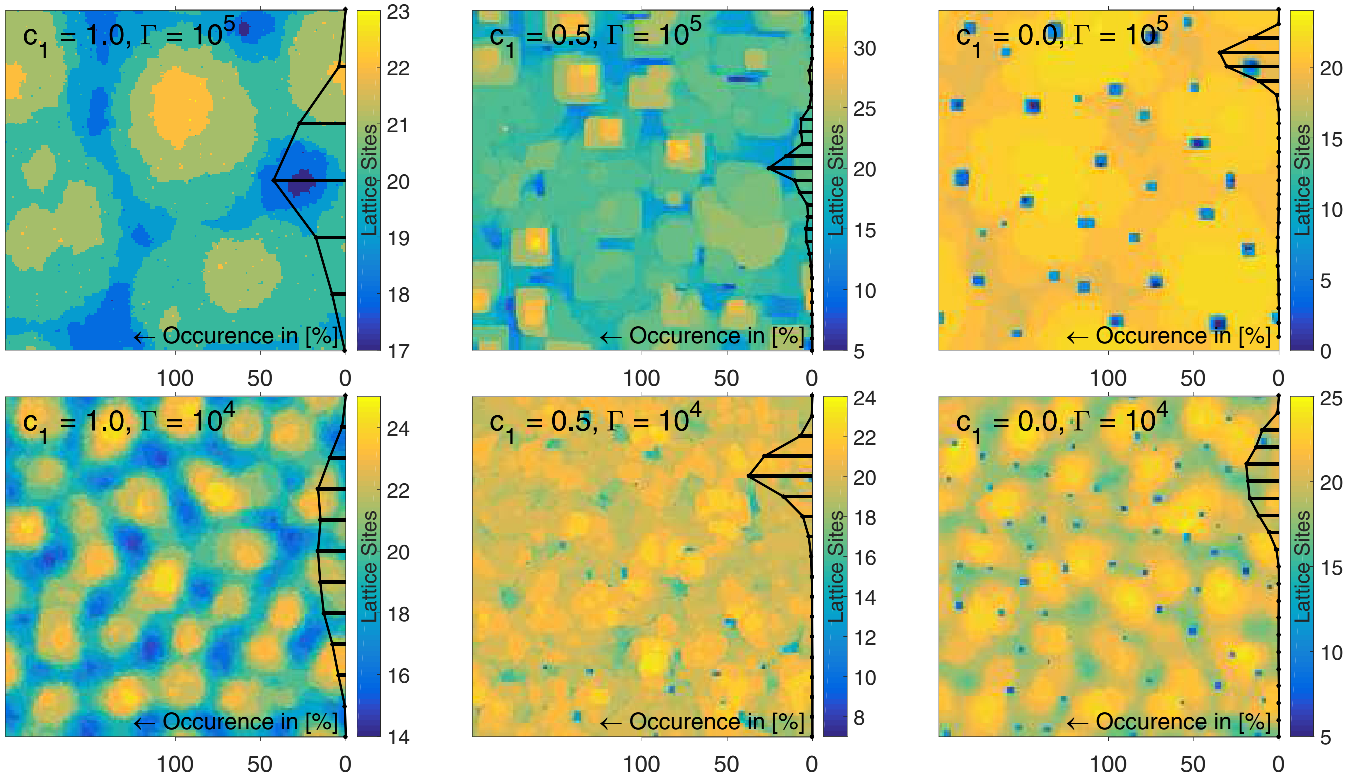

FIG. 7. Height maps of species 1 (CuPc, left), species 2 (C_{60}, right) and the 1:1 blend (middle), in which the concentration of species 1 is $c_1 = 0.5$, simulated at different ratios $\Gamma = 10^4$ (lower T, lower row) and $\Gamma = 10^5$ (higher T, upper row). The total amount of particles deposited on the 200 × 200 lattice was $20 \times (200)^2$, which corresponds to effectively 20 completely filled layers (≈20 nm).

needlelike crystals protruding from the thin films. It is difficult to observe such thin needles by AFM. Either the needles are bent downwards or they just break when the AFM-tip moves across them. In this case, the less invasive electron and ion scanning microscopy techniques are more suitable.

B. Evolution of roughness

Figure 10 shows the evolution of the roughness σ in the thin films grown at 310 K in comparison to the evolution of σ simulated at $\Gamma = 10^4$ (dotted lines) and 10^5 (solid lines). The corresponding experimental data sets of the blend and pure C_{60} at 400 K could not be evaluated due to lacking Kiessig oscillations, see Fig. 2. Furthermore, the roughness at 310 K can only be determined after the first Kiessig oscillations become visible, whereas the simulated value of σ is available from the beginning of growth. The experimental roughness is given in nanometers and the simulated roughness is given in units of layers. Depending on the particle species and the

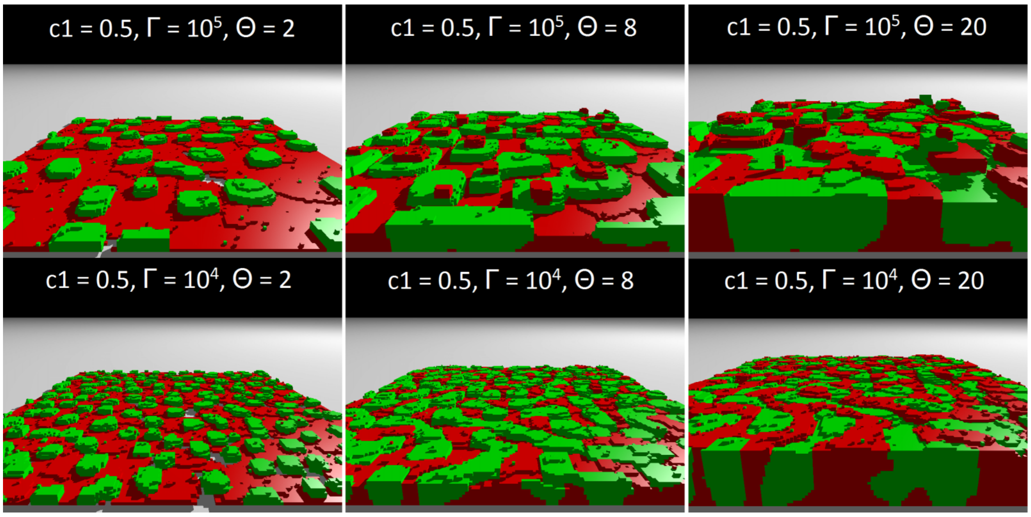

FIG. 8. Simulated snapshots on 200 × 200 lattice sites at a CuPc concentration of $c_1 = 0.5$ (red) and different ratios $\Gamma = 10^4$ and 10^5. The concentration of C_{60} is $c_2 = 1 - c_1$ (green). The total amount of deposited particles was $200 \times 200 \times \Theta$.

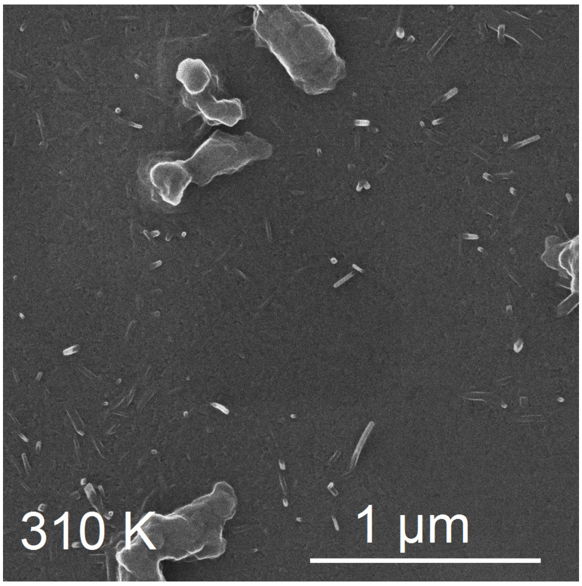

FIG. 9. Helium ion microscopy (HIM) image of a CuPc-C_{60} blend (ratio 1:1) grown at 2 Å/min and a substrate temperature of 310 K. The needlelike CuPc crystals protruding from the thin film are clearly recognizable.

crystallographic direction, the vertical distance between two layers varies. Along the (100) direction, the layer spacing is 0.7 nm for C_{60} and 1.3 nm for CuPc. In the blend, we have both types of molecules and one may simply assume an average height of 1.0 nm per layer. With this assumption, the computational and experimental results agree well, both qualitatively as well as quantitatively due to a suitable choice of interaction energies.

Figure 11 shows the post-growth roughness determined from AFM images of 20 nm thin films compared to the post-growth roughness determined from the simulated height profiles after deposition of 20 layers. Where feasible, the roughness was also determined from post-growth XRR. Contrary to the XRR measurements, which were acquired *in situ* directly after the growth, the AFM measurements were carried out *ex situ* several days after the growth making post-growth effects possible. Figure 10 shows that the evolution of roughness follows three different growth modes, initial layer-by-layer (LBL) growth followed by rapid roughening in the case of pure CuPc, rapid roughening from the beginning of growth in the case of pure C_{60} and 3D growth of varying degree for the blended thin films. In the following, these growth modes will be discussed in turn.

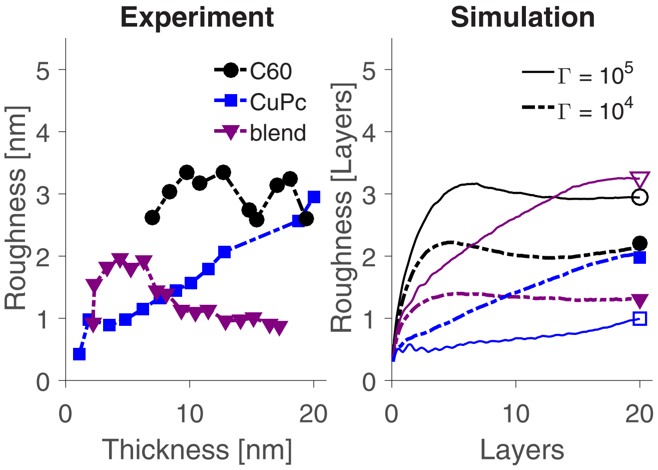

FIG. 10. Evolution of the root mean square roughness determined from the Kiessig oscillations in XRR at 310 K (left) and from simulations (right): dotted lines for $\Gamma = 10^4$ (lower T) and solid lines for $\Gamma = 10^5$ (higher T). Blue squares correspond to pure CuPc, black circles to pure C_{60}, and purple triangles to the 1:1 blend. One layer in the simulations corresponds to 0.7, 1.3, and 1 nm in the C_{60}, CuPc, and blend film, respectively.

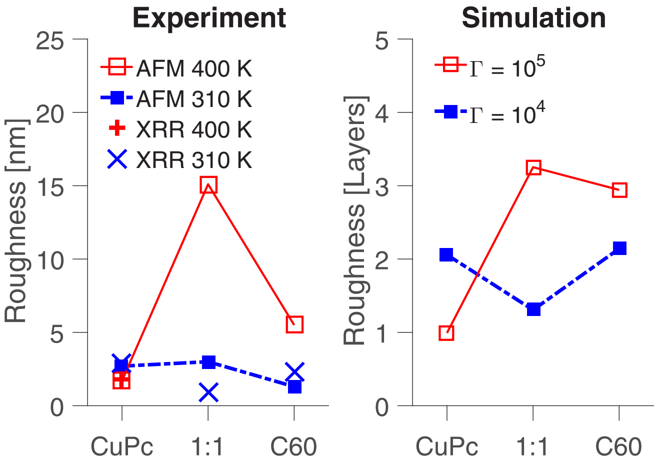

FIG. 11. Post-growth root mean square roughness σ determined from AFM images, XRR, and simulated height profiles at two different substrate temperatures: 310 K ($\Gamma = 10^4$) and 400 K ($\Gamma = 10^5$). One layer in the simulations corresponds to 0.7, 1.3, and 1 nm in the C_{60}, CuPc, and blend film, respectively.

C. CuPc

An alternating increase and decrease of roughness was observed during the simulated growth of the first few layers of species 1 (CuPc) at $\Gamma = 10^5$ (higher T) indicating LBL growth. Afterwards, the roughness of pure CuPc increases monotonously with time and thickness. At $\Gamma = 10^4$ (lower T), the roughening starts immediately without any oscillations and hence, no LBL growth occurs. It seems that the thickness after which the transition from LBL growth to rapid roughening happens can be increased by increasing the substrate temperature. In simulations of very large systems, ideal LBL growth does not occur. Instead, layer n starts to grow before layer $n-1$ beneath is completed, see Ref. [27] for investigations of a similar one-component model. The onset point n of roughening however depends on the diffusion to flux ratio Γ, the Ehrlich-Schwoebel barrier E^{ES} and also on the system size. Overall it is a complicated kinetic effect. Comparing the simulated data to our experiments, the monotonously growing roughness at larger thicknesses is confirmed. For a detailed evaluation of LBL growth, the temporal resolution of this experimental data set is too low. Experimental evidence for initial LBL growth can be found in prior studies on the thin film deposition of pentacene (PEN) [34], diindenoperylene

(DIP) [12,35–37] and fluorinated copper phthalocyanine (F_{16}-CuPc) [40]. In the present study, the post-growth roughness values determined from XRR and AFM agree well and deviate at most by 2 Å, see Fig. 11. The simulations result in a roughness of about 1 layer at $\Gamma = 10^5$ (higher T) and two layers at $\Gamma = 10^4$ (lower T). These values are in good quantitative agreement with the experiment considering a vertical layer spacing of 13 Å, which was previously determined by XRR. Notable is that the substrate temperature increase has a smoothing effect on the CuPc thin film, both in the experiment and in the simulation. Elevating the substrate temperature accelerates the downward diffusion of CuPc molecules and leads to smoother thin films [54]. The columnar growth of elongated CuPc crystals along the substrate supports the smoothing further [54].

D. C_{60}

The roughness of the C_{60} thin film increases rapidly in the beginning due to fast island formation and remains almost constant for the rest of film growth, see Fig. 10. The rapid increase of the roughness was reproduced computationally by the comparably weak C_{60}-substrate interaction leading to the formation of islands. A "dynamic wetting transition"[55] between initial LBL growth and island growth upon variation of ϵ_{sub} was found in the simulations for given ϵ and Γ. For the chosen C_{60}–C_{60} interaction $\epsilon = \epsilon_{22} = -3$ and an Ehrlich-Schwoebel barrier of $E^{\mathrm{ES}} = -3$, this transition occurs when $\epsilon_{\mathrm{sub}} < -2.44$ (for $\Gamma = 10^4$) and $\epsilon_{\mathrm{sub}} < -2.59$ (for $\Gamma = 10^5$), which is substantially smaller than the chosen C_{60}-substrate interaction of $\epsilon_{\mathrm{sub},2} = -1.0$. Without an Ehrlich-Schwoebel barrier ($E^{\mathrm{ES}} = 0$), the transition occurs at slightly weaker substrate potentials ($\epsilon_{\mathrm{sub}} < -2.31$ for $\Gamma = 10^4$ and $\epsilon_{\mathrm{sub}} < -2.52$ for $\Gamma = 10^5$). A small decrease of roughness arises after the initial roughening, both in the simulation and the experiment. It presumably stems from the coalescence of neighboring C_{60} islands leading to a slightly smoother film. In contrast to CuPc, the post-growth roughness of C_{60} thin films increases when the substrate is heated during growth. It was shown that C_{60} molecules react to substrate heating by island formation due to a molecular upward diffusion [39], which explains the enhanced roughness at 400 K found in the present study. This effect is well reproduced by the simulation, see Fig. 11. The deviation between the roughness determined from *ex-situ* AFM and from *in situ* XRR at 310 K amounts to 1 nm. Statistical variations and moderate post-growth effects may account for this deviation. The XRR-roughness of pure C_{60} and the blended thin film grown at 400 K are not available due to the missing Kiessig oscillations. The corresponding AFM values for C_{60} and the blend at 400 K are higher than the values simulated at $\Gamma = 10^5$, possibly because of stronger post-growth effects.

E. Blends

The roughness in blended CuPc-C_{60} thin films grown at 310 K increases rapidly in the beginning, decreases after the first five nanometers and falls considerably below the roughness of the pure component films (Fig. 10). This is a quite remarkable behavior but seems to be a more generic feature of blends [58]. In our simulations, the effect can be reproduced only with $E^{\mathrm{ES}}_{12} < E^{\mathrm{ES}}_{11[22]}$, i.e., smaller cross-species ES barrriers. Through the analysis of simulation snapshots at different stages of growth (see Fig. 8 in Sec. IV A), two competing processes can be observed at $\Gamma = 10^4$ (lower T). The nucleation of C_{60} islands increases the roughness in the beginning of growth while CuPc fills the gaps in between and smoothes out the corrugations. With the C_{60} domains expanding laterally, the space for CuPc is getting smaller and smaller. As a result, CuPc has to grow vertically until it reaches the height of C_{60} domains such that its smoothing impact finally prevails. However, the smoothing effect (as seen in the overall roughness) is less pronounced in the simulation compared to the experiment. Anisotropic intermolecular interactions that are not included in the simulation model may additionally contribute to the smoothing effect. Another growth scenario can be observed at 400 K. The missing Kiessig oscillations indicate a rapid roughening which remains during the entire growth. The more rapid roughening was confirmed by the simulation at $\Gamma = 10^5$. The solid line in Fig. 10 shows that the roughness of the blend is at first in between those of the pure species before increasing and finally becoming higher than the roughness of the pure films. The corresponding simulation snapshots in Fig. 8 of Sec. IV A explain this behavior by the tendency of particles to grow on top of domains of the respective other species, which compensates the above mentioned smoothing effect and makes the blended thin film even rougher. As a result of this, the post-growth roughness in Fig. 11 shows that unlike the remarkably smooth blend grown at 310 K, the roughness at 400 K exceeds the roughness of all other thin films both in the experimental and in the simulated data. The roughness determined from AFM is significantly larger than the roughness determined from the simulation and it is five times larger than the value determined from *in situ* XRR, which may be the result of a post-growth dewetting effect. The simulation ended when the deposition was finished without time for post-growth effects and the *in situ* XRR scans were carried out directly after the growth, whereas the AFM images where acquired *ex situ* several days after the growth.

F. Island densities and sizes

Figure 12 presents the island densities extracted from the AFM images and the simulated height maps (see Figs. 6 and 7 in Sec. IV A). There are approximately four times less islands per area in the pure thin films grown at 400 K than at 310 K. The island density at 400 K was found to be below 100 $\mu\mathrm{m}^{-2}$, whereas the number of islands reaches more than 400 $\mu\mathrm{m}^{-2}$ at 310 K for both pure CuPc and pure C_{60} thin films. Assuming a simple hexagonal distribution of islands, the interisland distance L would be $L = 1/\sqrt{n \sin(60^\circ)}$ with n being the density of islands and results in $L < 55$ nm at 310 K and $L > 100$ nm at 400 K. As mentioned earlier, the lateral sizes of coherently scattering domains determined from the width of GIXD peaks are much smaller indicating that each island consists of several crystallites with different orientations. Regarding the blended thin films, the size of coherently scattering domains goes down to less than 4 nm. However, there is no significant change of island densities in blended thin films compared to the pure films grown at 310 K. The island density stays

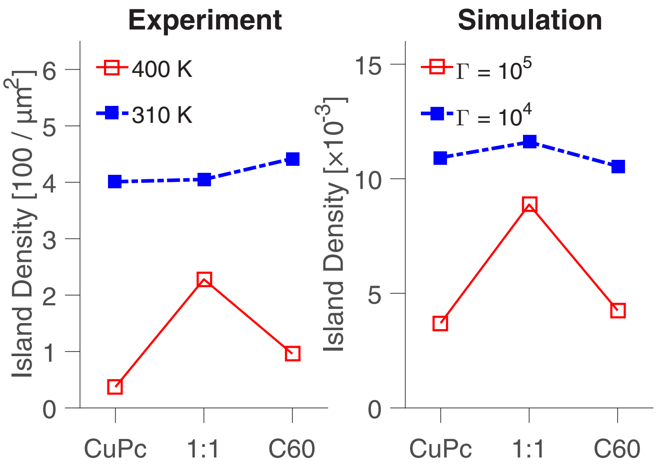

FIG. 12. Island densities determined from AFM images and from simulated height profiles at two different substrate temperatures: 310 K ($\Gamma = 10^4$) and 400 K ($\Gamma = 10^5$).

around 400 μm^{-2} and is mainly determined by the numerous tiny islands surrounding a few very tall islands (see Fig. 6 in Sec. IV A). The tall islands reach heights of more than 50 nm, but their contribution to the roughness and to the island density is low because of their rare occurrence. This behavior changes when raising the substrate temperature up to 400 K. The number of tall islands increases and their height reaches up to 100 nm. Regarding exclusively the density of tall islands which exceed a height of 50 nm, we find 1 μm^{-2} at 310 K and approximately 95 μm^{-2} at 400 K. The overall island density at 400 K is significantly larger than the island densities of the pure thin films grown at this temperature, both in the experiment and in the simulation. There is a good qualitative agreement between simulations and experiments. Solely, the absolute values differ. The experimentally observed tall islands at 310 K with their large mutual distances cannot be seen in simulations due to the limited substrate size of 200 × 200 lattice sites. Assuming that one lattice site corresponds to roughly 1 nm^2, the simulated height maps represent only 0.4% of the 3×3 μm^2 AFM images. The simulated island density of 0.009 per lattice site for the blend system at $\Gamma = 10^5$ corresponds then to 9000 μm^{-2}, which is almost two orders of magnitude higher. This is a consequence of the much lower value of Γ in comparison to experiment (although the simulated island density is much higher, the single-species roughness behavior is in semiquantitative agreement with the experiment due to an appropriate choice of E^{ES}). Besides the difference in the overall magnitude, the effect on the behavior of the island density due to demixing and due to temperature increase is captured very well qualitatively.

V. SUMMARY AND CONCLUSION

This study provides a detailed quantitative picture of thin film growth of CuPc-C_{60} blends. The experimental results are complemented by results from kinetic simulations of a generic, binary lattice model. We regard the CuPc-C_{60} blend as a model for a phase-separating system and abstain from all peculiarities of molecular shape and anisotropic interactions in the simulations. After initial layer-by-layer growth, rapid roughening was found in pure CuPc thin films, whereas the C_{60} thin films started to roughen at a very early stage of growth due to a fast formation of islands. It was shown that elevated substrate temperatures lead to larger islands at four times lower island densities. Furthermore, scanning electron and helium ion microscopy revealed needlelike islands protruding from the blended thin films. The simulations of the simple lattice model turned out to be well suited for understanding the influence of intermolecular interactions on the thin film growth and they were capable of reproducing and rationalizing the behavior of overall quantities such as the evolution of roughness and the island densities. Interaction parameters for the simulations were chosen in such a way that the growth modes in the simulations matched those of the pure species in the experiments, even though the parameters for deposition rate and the interaction energies were considerably off the experimental estimates. We performed simulations of the co-deposition of an island-forming particle species and a quasi-layer-by-layer growing particle species, which can be seen as analogous to C_{60} and CuPc, respectively. The introduction of a species-dependent Ehrlich-Schwoebel barrier led to films which were qualitatively similar to those observed in experiments. By increasing the diffusion-to-deposition ratio $\Gamma = D/F$ by a factor of 10 (which roughly corresponds to changing the substrate temperature from 310 K to 400 K), the following features were reproduced: (1) the blended film becomes rougher than the pure films, (2) the island density in the blended film is significantly higher than in the pure films, and (3) large islands (needles) start forming on top of the blended film. A similar mechanism might be responsible for the formation of large needles in experimental system. However, in these systems, we expect effects due to anisotropy, which cannot be captured in this model, to play an important role. In the simulations, we see that large islands of one species nucleate on top of a cluster of the respective other species leading to a pronounced roughness. Simulations in which we used either no or a species-independent ES barrier were unable to reproduce such a behavior indicating that this is a rationalization and model idealization of an effect which plays a role in actual film deposition experiments.

ACKNOWLEDGMENTS

We gratefully acknowledge the financial support of the German Research Foundation (Deutsche Forschungsgemeinschaft, DFG-Project GZ: OE 285/3-1, Grants No. SCHR 700/24-1 and No. SCHR 700/37-1; and HI XXX). We thank the P. Scherrer Institute for providing excellent facilities at the material science beamline MSX04SA of the Swiss Light Source and the European Synchrotron Radiation Facility for excellent facilities at the ID03 beamline. We thank R. Löffler and M. Turad for providing the helium ion microscope at the LISA+ center in Tübingen. G.D. gratefully acknowledges the Carl-Zeiss-Stiftung for support. M.H. further acknowledges the financial support of Alexander von Humboldt Foundation.

[1] S. R. Forrest, The path to ubiquitous and low-cost organic electronic appliances on plastic, Nature (London) **428**, 911 (2004).

[2] G. Witte and C. Wöll, Growth of aromatic molecules on solid substrates for applications in organic electronics, J. Mater. Res. **19**, 1889 (2004).

[3] F. Schreiber, Organic molecular beam deposition: Growth studies beyond the first monolayer, Phys. Stat. Sol. (a) **201**, 1037 (2004).

[4] A. Hinderhofer and F. Schreiber, Organic-organic heterostructures: Concepts and applications, ChemPhysChem **13**, 628 (2012).

[5] A. Opitz, J. Wagner, W. Brütting, I. Salzmann, N. Koch, J. Manara, J. Pflaum, A. Hinderhofer, and F. Schreiber, Charge separation at molecular donor-acceptor interfaces: Correlation between morphology and solar cell performance, IEEE J. Sel. Top. Quant. **16**, 1707 (2010).

[6] U. Hörmann, C. Lorch, A. Hinderhofer, A. Gerlach, M. Gruber, J. Kraus, B. Sykora, S. Grob, T. Linderl, A. Wilke, A. Opitz, R. Hansson, A. S. Anselmo, Y. Ozawa, Y. Nakayama, H. Ishii, N. Koch, E. Moons, F. Schreiber, and W. Brütting, V_{OC} from a morphology point of view: the influence of molecular orientation on the open circuit voltage of organic planar heterojunction solar cells, J. Phys. Chem. C **118**, 26462 (2014).

[7] K. Broch, J. Dieterle, F. Branchi, N. J. Hestand, Y. Olivier, H. Tamura, C. Cruz, V. M. Nichols, A. Hinderhofer, D. Beljonne, F. C. Spano, G. Cerullo, C. J. Bardeen, and F. Schreiber, Robust singlet fission in pentacene thin films with tuned charge transfer interactions, Nat. Commun. **9**, 954 (2018).

[8] F. Anger, J. O. Ossó, U. Heinemeyer, K. Broch, R. Scholz, A. Gerlach, and F. Schreiber, Photoluminescence spectroscopy of pure pentacene, perfluoropentacene, and mixed thin films, J. Chem. Phys. **136**, 054701 (2012).

[9] S. Veenstra, G. Malliaras, H. Brouwer, F. Esselink, V. Krasnikov, P. van Hutten, J. Wildeman, H. Jonkman, G. Sawatzky, and G. Hadziioannou, Sexithiophene-C_{60} blends as model systems for photovoltaic devices, Synth. Met. **84**, 971 (1997).

[10] C. Lorch, K. Broch, V. Belova, G. Duva, A. Hinderhofer, A. Gerlach, M. Jankowski, and F. Schreiber, Growth and annealing kinetics of α-sexithiophene and fullerene C_{60} mixed films, J. Appl. Crystallogr. **49**, 1266 (2016).

[11] R. Banerjee, J. Novák, C. Frank, C. Lorch, A. Hinderhofer, A. Gerlach, and F. Schreiber, Evidence for Kinetically Limited Thickness Dependent Phase Separation in Organic Thin Film Blends, Phys. Rev. Lett. **110**, 185506 (2013).

[12] C. Lorch, J. Novák, R. Banerjee, S. Weimer, J. Dieterle, C. Frank, A. Hinderhofer, A. Gerlach, F. Carla, and F. Schreiber, Influence of C_{60} co-deposition on the growth kinetics of diindenoperylene - From rapid roughening to layer-by-layer growth in blended organic films, J. Chem. Phys. **146**, 052807 (2017).

[13] I. Salzmann, S. Duhm, R. Opitz, R. L. Johnson, J. P. Rabe, and N. Koch, Structural and electronic properties of pentacene-fullerene heterojunctions, J. Appl. Phys. **104**, 114518 (2008).

[14] S. Heutz, P. Sullivan, B. Sanderson, S. Schultes, and T. Jones, Influence of molecular architecture and intermixing on the photovoltaic, morphological and spectroscopic properties of CuPc-C_{60} heterojunctions, Sol. Energ. Mat. Sol. Cells **83**, 229 (2004).

[15] P. Sullivan, S. Heutz, S. M. Schultes, and T. S. Jones, Influence of codeposition on the performance of CuPc-C_{60} heterojunction photovoltaic devices, Appl. Phys. Lett. **84**, 1210 (2004).

[16] J. Krug, P. Politi, and T. Michely, Island nucleation in the presence of step-edge barriers: Theory and applications, Phys. Rev. B **61**, 14037 (2000).

[17] T. Michely and J. Krug, *Islands, Mounds, and Atoms. Patterns and Processes in Crystal Growth Far from Equilibrium* (Springer, Berlin, 2004).

[18] M. Kardar, G. Parisi, and Y. Zhang, Dynamic Scaling of Growing Interfaces, Phys. Rev. Lett. **56**, 889 (1986).

[19] M. Kardar, Roughness and ordering of growing films, Physica A **281**, 295 (2000).

[20] L. Muccioli, G. D'Avino, and C. Zannoni, Simulation of vapor-phase deposition and growth of a pentacene thin film on C_{60}(001), Adv. Mater. **23**, 4532 (2011).

[21] O. M. Roscioni, G. D'Avino, L. Muccioli, and C. Zannoni, Pentacene crystal growth on silica and layer-dependent step-edge barrier from atomistic simulations, J. Phys. Chem. Lett. **9**, 6900 (2018).

[22] S. Chiodini, G. D'Avino, L. Muccioli, L. Bartolini, D. Gentili, S. Toffanin, and C. Albonetti, Self-organization of complete organic monolayers via sequential post-deposition annealing, Prog. Org. Coat. **138**, 105408 (2020).

[23] M. Einax, W. Dieterich, and P. Maass, Colloquium: Cluster growth on surfaces: Densities, size distributions, and morphologies, Rev. Mod. Phys. **85**, 921 (2013).

[24] P. Šmilauer and D. D. Vvedensky, Coarsening and slope evolution during unstable spitaxial growth, Phys. Rev. B **52**, 14263 (1995).

[25] M. Siegert and M. Plischke, Formation of pyramids and mounds in molecular beam epitaxy, Phys. Rev. E **53**, 307 (1996).

[26] F. F. Leal, T. J. Oliveira, and S. C. Ferreira, Kinetic modelling of epitaxial film growth with up- and downward step barriers, J. Stat. Mech. (2011) P09018.

[27] T. A. d. Assis and F. D. A. Aarão Reis, Dynamic scaling and temperature effects in thin film roughening, J. Stat. Mech. (2015) P06023.

[28] D. Landau, S. Pal, and Y. Shim, Monte carlo simulations of film growth, Comput. Phys. Commun. **121-122**, 341 (1999).

[29] X. Tao, Y. Shim, and D. Landau, Monte carlo simulation of film growth in a phase separating binary alloy model, Physica A **387**, 2495 (2008).

[30] K. A. Ritley, B. Krause, F. Schreiber, and H. Dosch, A portable ultrahigh vacuum organic molecular beam deposition system for *in situ* x-ray diffraction measurements, Rev. Sci. Instrum. **72**, 1453 (2001).

[31] B. Krause, F. Schreiber, H. Dosch, A. Pimpinelli, and O. H. Seeck, Temperature dependence of the 2D-3D transition in the growth of PTCDA on Ag(111): A real-time x-ray and kinetic monte carlo study, Europhys. Lett. **65**, 372 (2004).

[32] B. Krause, A. C. Dürr, F. Schreiber, H. Dosch, and O. H. Seeck, Late growth stages and post-growth diffusion in organic epitaxy: PTCDA on Ag(111), Surf. Sci. **572**, 385 (2004).

[33] P. R. Willmott, D. Meister, S. J. Leake, M. Lange, A. Bergamaschi, M. Böge, M. Calvi, C. Cancellieri, N. Casati, A. Cervellino, Q. Chen, C. David, U. Flechsig, F. Gozzo, B. Henrich, S. Jäggi-Spielmann, B. Jakob, I. Kalichava, P.

Karvinen, J. Krempasky, A. Lüdeke, R. Lüscher, S. Maag, C. Quitmann, M. L. Reinle-Schmitt, T. Schmidt, B. Schmitt, A. Streun, I. Vartiainen, M. Vitins, X. Wang, and R. Wullschleger, The Materials Science beamline upgrade at the Swiss Light Source, J. Synchrotron Radiat. **20**, 667 (2013).

[34] S. Kowarik, A. Gerlach, W. Leitenberger, J. Hu, G. Witte, C. Wöll, U. Pietsch, and F. Schreiber, Energy-dispersive X-ray reflectivity and GID for real-time growth studies of pentacene thin films, Thin Solid Films **515**, 5606 (2007).

[35] S. Kowarik, A. Gerlach, M. W. A. Skoda, S. Sellner, and F. Schreiber, Real-time studies of thin film growth: Measurement and analysis of x-ray growth oscillations beyond the anti-Bragg point, Eur. Phys. J. Special Topics **167**, 11 (2009).

[36] A. C. Dürr, F. Schreiber, K. A. Ritley, V. Kruppa, J. Krug, H. Dosch, and B. Struth, Rapid Roughening in Thin Film Growth of an Organic Semiconductor (diindenoperylene), Phys. Rev. Lett. **90**, 016104 (2003).

[37] X. Zhang, E. Barrena, D. de Oteyza, and H. Dosch, Transition from layer-by-layer to rapid roughening in the growth of DIP on SiO_2, Surf. Sci. **601**, 2420 (2007).

[38] S. Bommel, N. Kleppmann, C. Weber, H. Spranger, P. Schäfer, J. Novák, S. Roth, F. Schreiber, S. Klapp, and S. Kowarik, Unravelling the multilayer growth of the fullerene C_{60} in real time, Nat. Commun. **5**, 5388 (2014).

[39] S. Bommel, H. Spranger, C. Weber, N. Kleppmann, S. V. Roth, S. H. L. Klapp, and S. Kowarik, Thermally-activated post-growth dewetting of fullerene C_{60} on mica, Phys. Status Solidi RRL **9**, 646 (2015).

[40] J. Yang, S. Yim, and T. S. Jones, Molecular-orientation-induced rapid roughening and morphology transition in organic semiconductor thin-film growth, Sci. Rep. **5**, 9441 (2015).

[41] G. Duva, L. Pithan, A. Gerlach, A. Janik, A. Hinderhofer, and F. Schreiber, Roughness evolution in strongly interacting donor: acceptor mixtures of molecular semiconductors. An in situ real-time growth study using x-ray reflectivity, J. Phys.: Condens. Matter **33**, 115003 (2021).

[42] M. Björck and G. Andersson, GenX: An extensible X-ray reflectivity refinement program utilizing differential evolution, J. Appl. Cryst. **40**, 1174 (2007).

[43] A. Hoshino, Y. Takenaka, and H. Miyaji, Redetermination of the crystal structure of α-copper phthalocyanine grown on KCl, Acta Cryst. B **59**, 393 (2003).

[44] M. Ashida, N. Uyeda, and E. Suito, Unit cell metastable-form constants of various phthalocyanines, Bull. Chem. Soc. Jpn. **39**, 2616 (1966).

[45] W. I. F. David, R. M. Ibberson, J. C. Matthewman, K. Prassides, T. J. S. Dennis, J. P. Hare, H. W. Kroto, R. Taylor, and D. R. M. Walton, Crystal structure and bonding of ordered C_{60}, Nature (London) **353**, 147 (1991).

[46] J. L. de Boer, S. van Smaalen, V. Petricek, M. Dusek, M. A. Verheijen, and G. Meijer, Hexagonal close-packed C_{60}, Chem. Phys. Lett. **219**, 469 (1994).

[47] A. Hinderhofer, A. Gerlach, K. Broch, T. Hosokai, K. Yonezawa, K. Kato, S. Kera, N. Ueno, and F. Schreiber, Geometric and electronic structure of templated C_{60} on diindenoperylene thin films, J. Phys. Chem. C **117**, 1053 (2013).

[48] A. Patterson, The Scherrer Formula of X-ray particle size determination, Phys. Rev. **56**, 978 (1939).

[49] See Supplement Material at http://link.aps.org/supplemental/10.1103/PhysRevMaterials.5.045601 for additional figures.

[50] C. Schünemann, D. Wynands, L. Wilde, M. Hein, S. Pfützner, C. Elschner, K.-J. Eichhorn, K. Leo, and M. Riede, Phase separation analysis of bulk heterojunctions in small-molecule organic solar cells using zinc-phthalocyanine and C_{60}, Phys. Rev. B **85**, 245314 (2012).

[51] F. W. Karasek and J. C. Decius, Observations concerning polymorphic crystalline modifications of the phthalocyanines, J. Am. Chem. Soc. **74**, 4716 (1952).

[52] E. Suito, N. Uyeda, and M. Ashida, Epitaxial growth of condensed aromatic polycyclic compounds, Nature (London) **194**, 273 (1962).

[53] T. Nonaka, Y. Nakagawa, Y. Mori, M. Hirai, T. Matsunobe, M. Nakamura, T. Takahagi, A. Ishitani, H. Lin, and K. Koumoto, Epitaxial growth of α-copper phthalocyanine crystal on Si(001) substrate by organic molecular beam deposition, Thin Solid Films **256**, 262 (1995).

[54] B. Reisz, V. Belova, G. Duva, C. Zeiser, M. Hodas, J. Hagara, P. Siffalovic, L. Pithan, T. Hosokai, A. Hinderhofer, A. Gerlach, and F. Schreiber, Polymorphism and structure formation in copper phthalocyanine thin films, J. Appl. Cryst. **54**, 203 (2021), (in print).

[55] E. Empting, M. Klopotek, A. Hinderhofer, F. Schreiber, M. Oettel, Lattice gas study of thin-film growth scenarios and transitions between them: Role of substrate, Phys. Rev. E **103**, 023302 (2021).

[56] V. R. Barlett, J. Bigeón, M. Hoyuelos, and H. Mártin, Differences between fixed time step and kinetic monte carlo methods for biased diffusion, J. Comput. Phys. **228**, 5740 (2009).

[57] O. Berger, W.-J. Fischer, B. Adolphi, S. Tierbach, V. Melev, and J. Schreiber, Studies on phase transformations of Cu-phthalocyanine thin films, J. Mater. Sci. Mater. Electron. **11**, 331 (2000).

[58] A. Hinderhofer, J. Hagenlocher, A. Gerlach, J. Krug, M. Oettel, and F. Schreiber, Non-equilibrium roughness evolution of small molecule mixed films reflecting equilibrium phase behavior, arXiv:2103.04754v1.